Geophysical Research Letter

Supporting Information for

A sharp structural boundary in lowermost mantle beneath Alaska detected by core phase differential travel times for the anomalous South Sandwich Islands to Alaska Path

Xin Long, Hitoshi Kawakatsu, Nozomu Takeuchi

Earthquake Research Institute, The University of Tokyo

Contents of this file

Introduction

The supporting information includes a table (Table S1) of earthquakes used in this research and some supplementary figures. Figure S1 shows the projection of the inner-core paths for earthquakes (evt1, evt2 and evt3) analyzed in the main text. Figure S2 shows the stations and PKP piercing points corresponding to the "initial" and "kink part" of the residual pattern. Figure S3 shows the observed and modeled PKPdf/PKPbc amplitude ratios. Figure S4 shows the comparison between observed and predicted absolute PKPbc-df residuals. Figure S5 shows the location of PKPdf piercing points for evt1, evt2 and evt3 within different azimuth corridors. Figure S6 shows the PKPbc-df residuals for event 2016/07/13 within different azimuth corridors. Figure S7 shows PKPbc-df residuals for event 2014/06/13 at South Mid-Atlantic Ridge. Figure S8 shows tests for other models. Figure S9 shows synthetic seismograms for the background model and the Model 2 in Figure 2b. Figure S10 shows data and modeling results for other 4 events in Table S1. Figure S11 shows prediction of several anisotropy models. Figure S12 shows PKPbc-df residual predicted by different models of discontinuity in the upper inner core. Figure S13 is a schematic figure that shows the geometry for the modeling.

Table S1. Earthquakes used in this research

Event Date	Lat. (°)	Lon. (°)	Depth (km)	Mag (Mw)	Region
2016/08/21 (evt1)	-55.27	-31.75	10.0	6.4	SSI
2016/08/02 (evt3)	-58.72	-25.61	35.0	5.5	SSI
2016/07/31	-56.25	-27.55	98.2	5.9	SSI
2016/05/28 (evt2)	-56.24	-26.93	78	7.2	SSI
2016/02/18	-56.21	-27.62	119.3	5.8	SSI
2015/09/30	-56.19	-27.71	101	5.7	SSI
2014/05/17	-56.24	-27.53	90	5.5	SSI
2014/02/01	-56.83	-27.34	130.0	6.1	SSI
2011/12/11	-56.05	-28.21	139.6	6.3	SSI
2014/06/13	-46.03	-13.88	6.4	5.8	Southern Mid-Atlantic Ridge

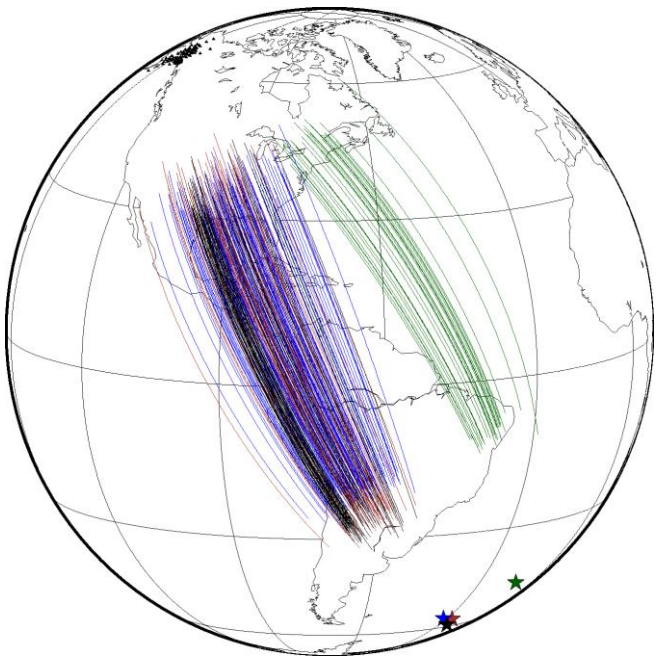

Figure S1. Locations of event 2016/08/21 (evt1, blue star), 2016/08/02 (black star), 2016/05/28 (evt2, brown star) and 2014/06/13 (evt3, green star), and projection of the ray paths in the inner core.

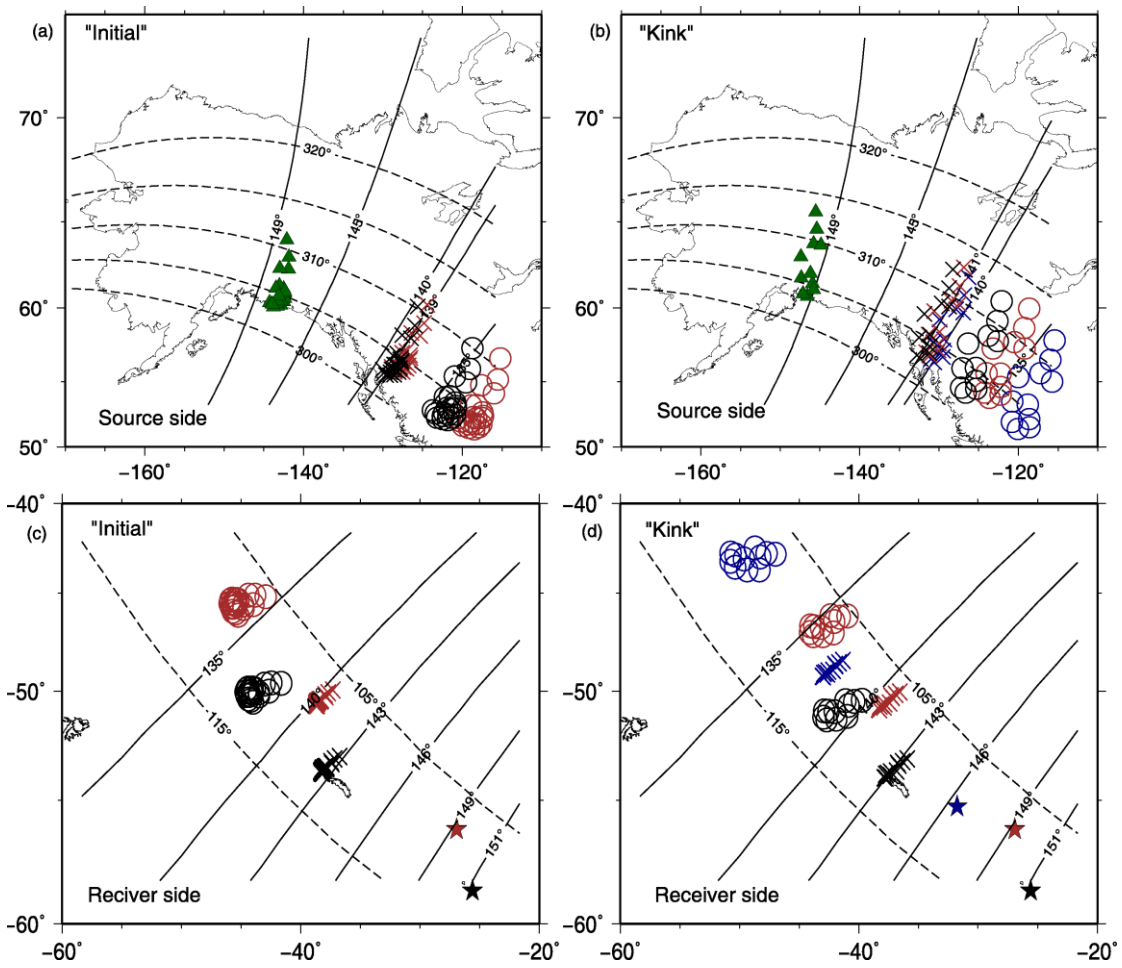

Figure S2. Piercing points of PKPdf and PKPbc at the receiver side that correspond to the "initial" (a) and "kink" (b) parts of the residual pattern (Figure 1c) for evt1, evt2 and evt3. Green triangles show station locations, and crosses and circles respectively denote PKPdf and PKPbc piercing points (different colors correspond to those events shown in Figure 1f with the same colors). Solid line and broken lines indicate distance and azimuth contours for evt2. Linear feature of stations and piercing points subparallel to the distant contours can be seen. Symbols in (c) and (d) are the same as (a) and (b), but are plotted at the source side for "initial" and "kink" parts, and the contours are for station KLU. Stars are earthquakes.

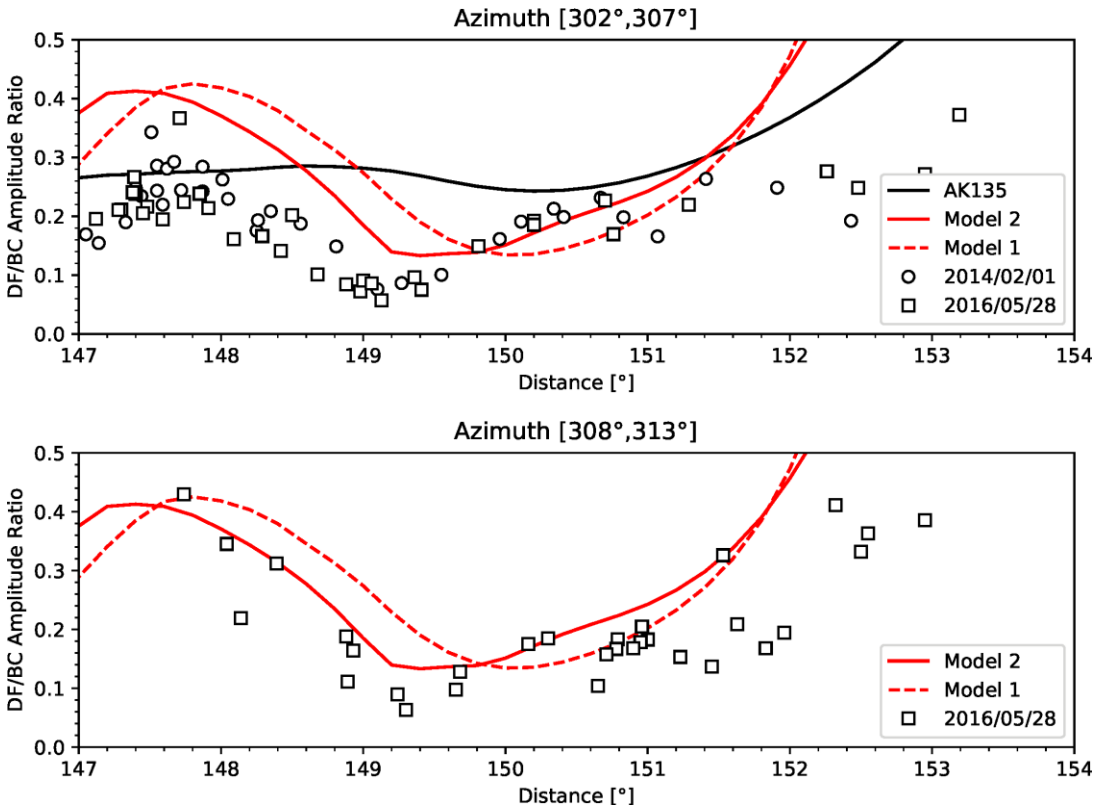

Figure S3. Observed and modeled (for models 1 and 2 in Figure 2b) PKPdf/PKPbc amplitude ratios. For evt2, data within different azimuth range are shown, and they are basically consistent. It could be seen that Model 2 predicts the observed minimum of PKPdf/PKPbc amplitude ratio better than Model 1 and AK135.

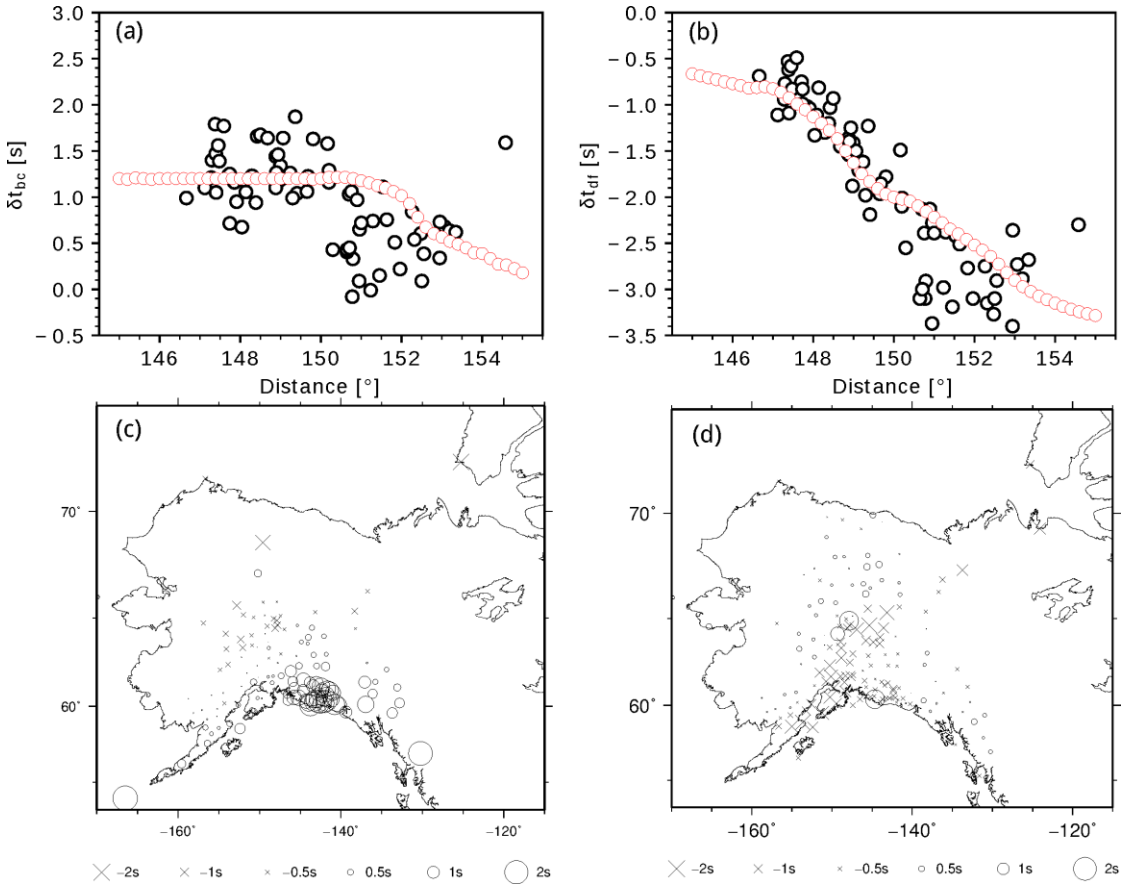

Figure S4. Synthetic PKPdf and PKPbc residuals are compared with observation for evt2, and they are basically consistent except at distance larger than 150°. This may be due to high velocity heterogeneity at upper mantle beneath Central Alaska. (a), (b): Black open circles show PKPbc and PKPdf residuals relative to ak135 for evt2, and red circles are those predicted by Model 2 in Figure 2b. (c), (d): P residuals relative to ak135 for two earthquakes, one in central America (2016/06/15) and the other near Japan (2016/11/23). A relative delay of P wave in central Alaska could be seen. This may explain why the synthetic absolute residuals do not fit data well at large distances (>~150°).

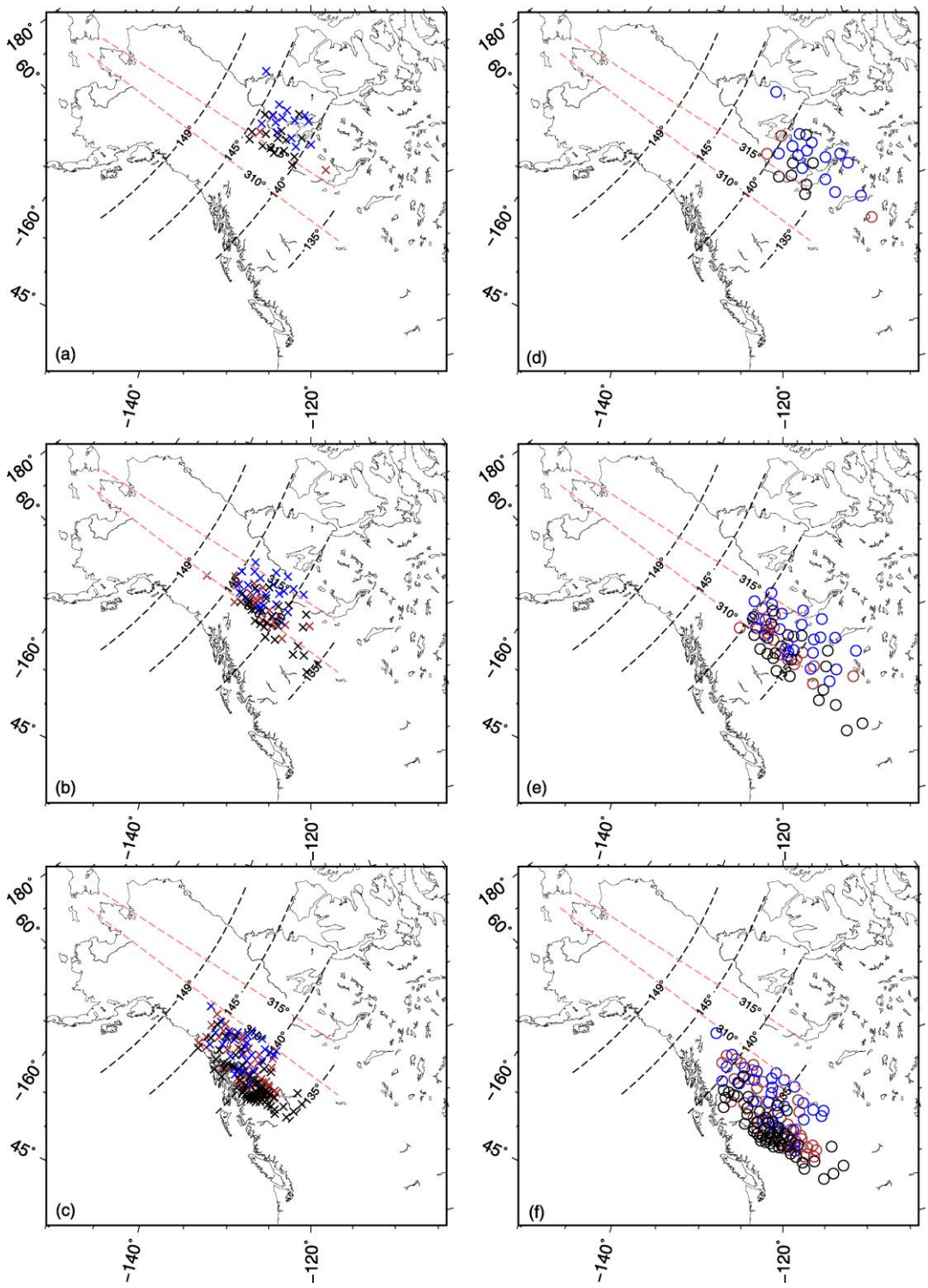

Figure S5. Piercing points of PKPdf (a, b, c) and PKPbc (d, e, f) for data of evt1 (blue colors), evt2 (brown) and evt3 (black) shown in Figure 3, and they are roughly divided into the 3 azimuth corridors. (a,d), (b,e) and (c,f) respectively correspond to columns 3, 2, and 1 in Figure 3,. Black and red dashed lines are distance and azimuth contours for evt2.

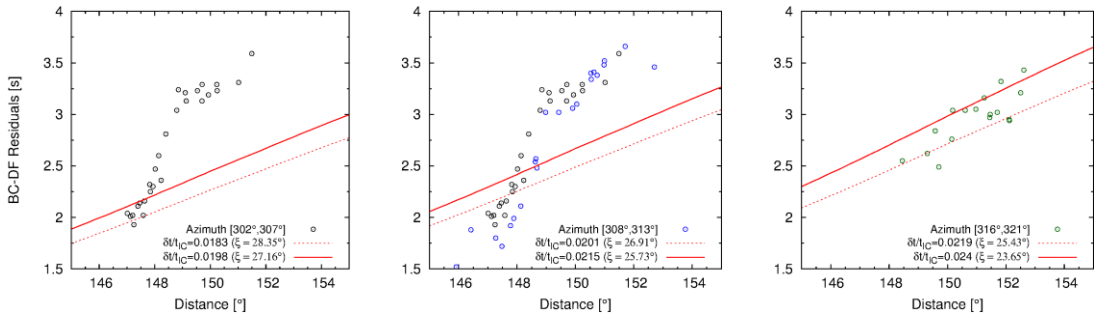

Figure S6. PKPbc-df residuals for event 2016/07/31 in the main SSI group. Data are divided into 3 corridors as that in Figure 3. This is shown just as supplement.

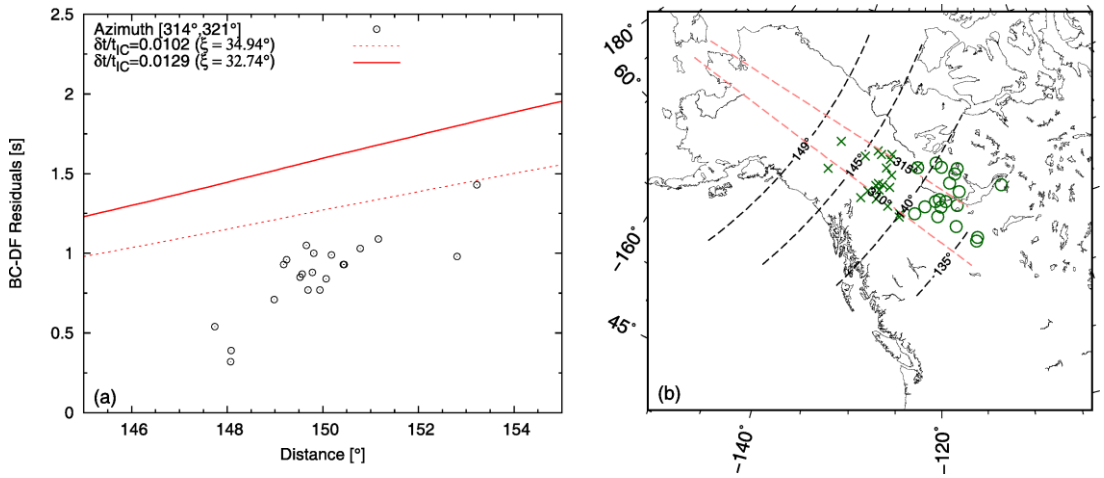

Figure S7. (a) PKPbc-df residuals for the event 2014/06/13 at South Mid-Atlantic Ridge. Only data confined in the 2nd corridor in Figure S4 are shown. (b) PKPdf (cross) and PKPbc (circle) piercing points for data in (a).

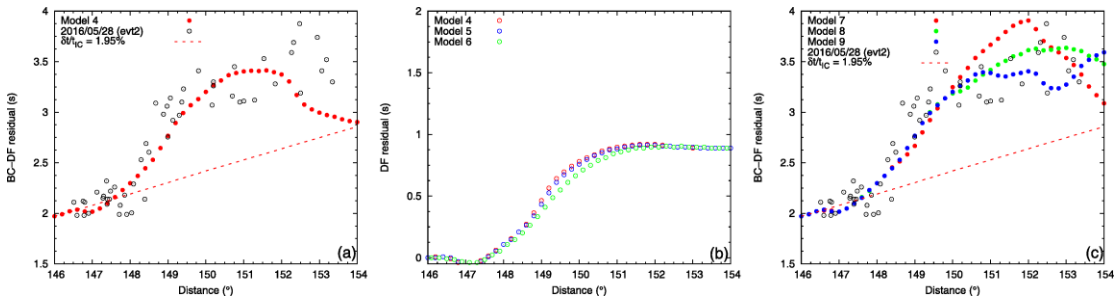

Figure S8. Tests with additional models to those in Figure 2b. Model 4, 5 and 6 has a constant height (400km) layer with 3% δV_p, and in Model 5 and 6, the velocity perturbation increases gradually from 0 to 3% within 50 and 100km from the boundary. Thickness variations are added into Model 7, 8, and 9. For those models, velocity perturbation is constant (3%), and thickness has a step change from 400 to 700km at 200, 250 and 300km away from the boundary. (a) PKPbc-df residuals for Model 4. It suggests a constant heterogeneity layer can explain the steep increase of the residual, but the residual would drop quickly at distance larger than 151°, which is

not consistent with the data. (b) PKPdf residuals for Model 4, 5 and 6. Residual patterns for these models are shifted to make starting point of them to coincide. It could be seen that PKPdf is not very sensitive to the sharpness of the boundary, even though PKPdf residuals increase more gradually if the boundary becomes less sharp. (c) PKPbc-df residuals for Model 7, 8 and 9. It shows that increase of the layer thickness is also acceptable to explain the PKPbc-df residuals at large distances.

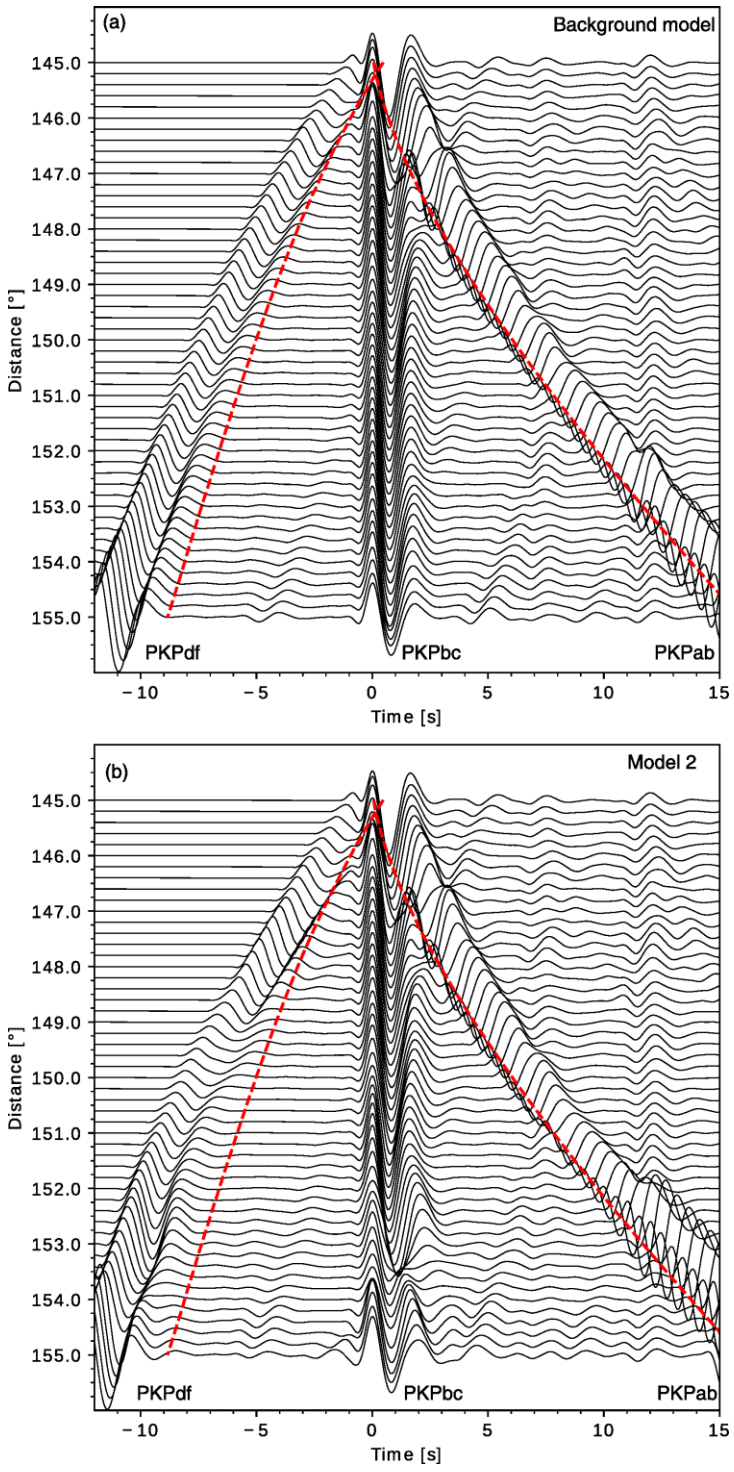

Figure S9. Synthetic seismograms for (a) background model and (b) Model 2 in Figure 2b. Red line show the travel time prediction of AK135. An isotropic source with a depth of 100km is used. Each trace is normalized by its maximum amplitude. It could be seen that PKPab in (a) an (b) are different at distance larger than 151°. It is the delay of PKPab relative to PKPbc that causes the shift of the waveform (compared with red lines that are the same in (a) and (b)).

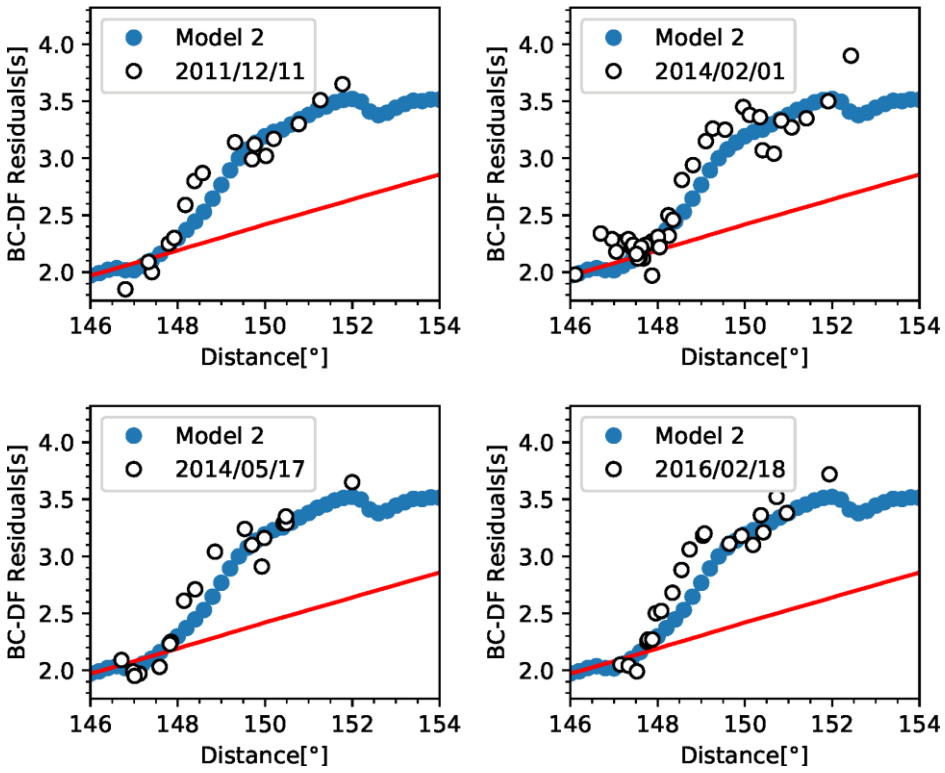

Figure S10. Data for other 4 events in Table S1, and the prediction of Model 2 is plotted for comparison. Red line stands for fractional residual of 1.95%, and data are confined within the azimuth corridor 1.

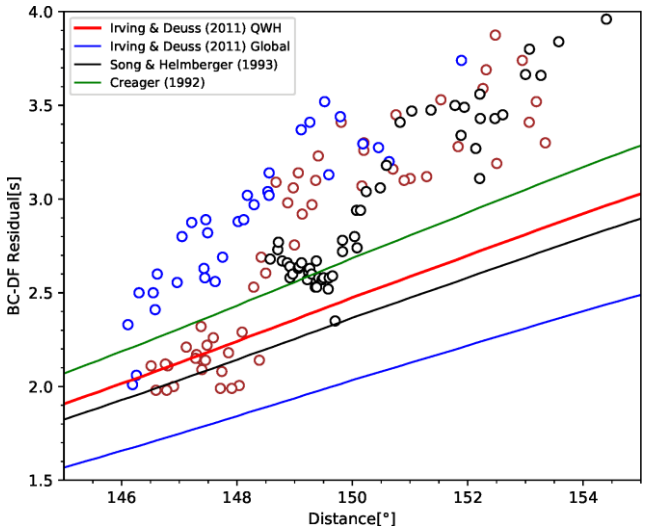

Figure S11. PKPbc-df residual predicted by several anisotropy models of inner core for $\boldsymbol{\xi = 27°}$. Each model gives different strength of anisotropy. Irving & Deuss (2011) QWH: 4.8%; Irving & Deuss (2011) Global: 3.8%; Song & Helmberger (1993): 3%; Creager (1992): 3.5%.

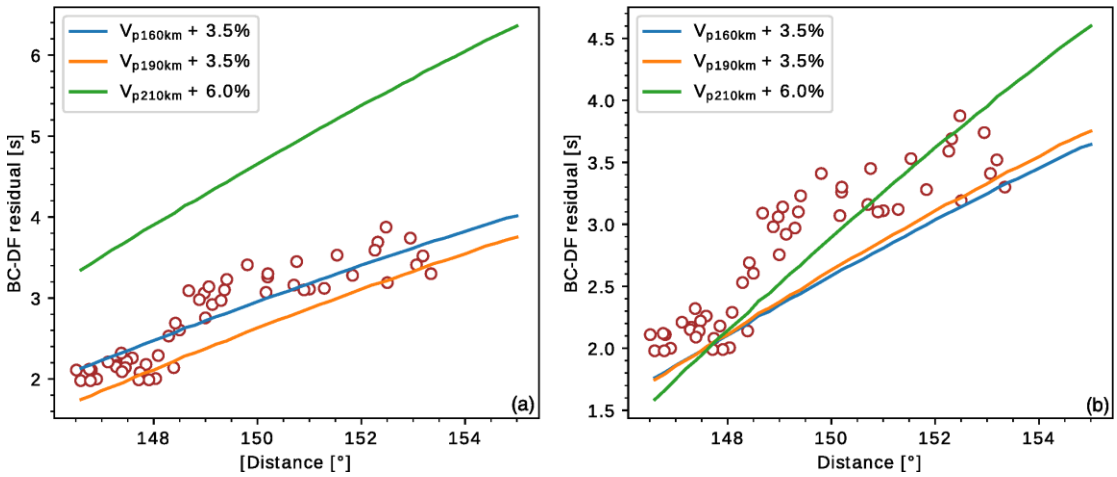

Figure S12. (a) PKPbc-df residual predicted by different models of discontinuity in the upper inner core. Data for evt2 is plotted for comparison (brown circles). Lines represent predictions for discontinuities with different depths beneath the inner-outer core boundary, and velocity jumps with respect to AK135. (b) the same as (a) but baselines are shifted for the models with discontinuities at 160km and 210km beneath the inner-outer boundary. This is to show the effect of the velocity jump for the increase of the residuals. Note that the green line corresponding a jump of 6% still does not produce the sharp increase observed in data.

Modeling Details

The dominant frequency for the modeling is 1Hz in this study, and an isotropic source is used for simplicity. In AxiSEM, the size and location of a heterogeneity block are defined by it upper and lower boundary (radius and colatitude), and the heterogeneity is axisymmetric relative to the source that we place on the symmetry axis.

In the modeling, we set the symmetry axis of the inner core anisotropy and the ray paths in the same meridian plane, which is different from the real situation. Then, for a given epicentral distance, ξ in the modeling is not the same as that for the real source-receiver geometry (e.g., for a distance of 148°, ξ is about 16°, but the real ξ is around 26° as we mentioned earlier). However, under the assumption of equation (2), we can make a good approximation by setting the symmetry axis of the inner core anisotropy 10° tilted relative to the Earth's rotation axis in AxiSEM (Figure S13). The effects due to the background model with the anisotropic inner core finally turn out to be almost canceled, and the detail of modeling (e.g., the introduction of tilt) does not change the result significantly.

In the actual simulation, AxiSEM always rotates the source to the north pole, and the positions of the heterogeneity and receivers are also changed accordingly. In the currently available version of the software (version 1.1), the anisotropy axis of the

inner core is defined in terms of the symmetry axis, and kept 10 °tilted relative to it in our simulation. As a result, geometry for modeling is always as such showed in Figure S13. For example, for evt2, we set the source latitude and the lower boundary of the heterogeneity to be 88 °and 145 °respectively in the input file, then AxiSEM rotates the source and the boundary to 90 °and 143 °respectively in the actual simulation. Then the distance from source to the heterogeneity is 143 °.

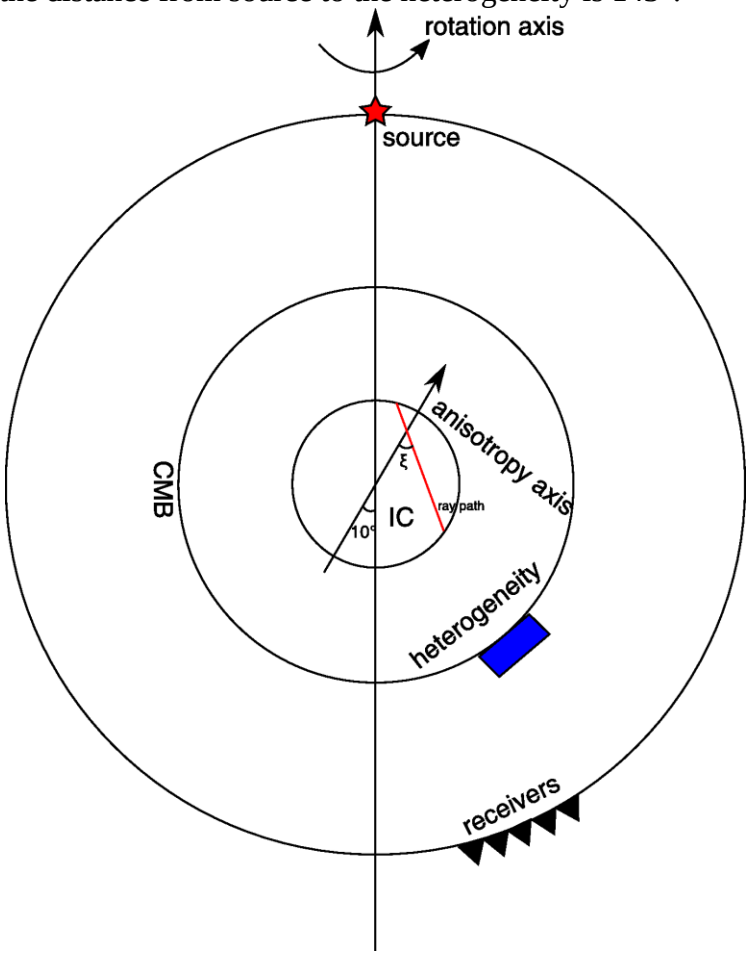

Figure S13. A schematic figure that shows the geometry for the modeling. The red line is the ray segment in the inner core, and ξ is the angle between the ray segment and the anisotropy axis.